APPENDIX

Table 3. *Cartesian forms for the real spherical harmonic functions with $l = 8$ (Paturle, 1990)*

These extend the published tabulation for $l \leq 7$ (Paturle & Coppens, 1988). The arguments x, y and z are orthonormal components, *i.e.* direction cosines, of a unit vector and the functions

$$y_{l,m} = N_{l,|m|} C_{l,|m|} c_{l,m}(x,y,z)$$

are normalized such that

$$\int_{\Omega} |y_{l,m}| \mathrm{d}\Omega = 2 - \delta_{0,l}.$$

m	$c_{8,m}$	$C_{8,\|m\|}$	$N_{8,\|m\|}$
0	$6435z^8 - 12012z^6 + 6930z^4 - 1260z^2 + 35$	0.0078125	0.0059609
1	$(715z^7 - 1001z^5 + 385z^3 - 35z)x$	0.5625	0.0784858
−1	$(715z^7 - 1001z^5 + 385z^3 - 35z)y$		
2	$(143z^6 - 143z^4 + 33z^2 - 1)(x^2 - y^2)$	19.6875	0.3253786
−2	$(143z^6 - 143z^4 + 33z^2 - 1)(2xy)$		
3	$(39z^5 - 26z^3 + 3z)(x^3 - 3xy^2)$	433.125	0.8780415
−3	$(39z^5 - 26z^3 + 3z)(3x^2y - y^3)$		
4	$(65z^4 - 26z^2 + 1)(x^4 - 6x^2y^2 + y^4)$	1299.375	0.3411683
−4	$(65z^4 - 26z^2 + 1)(4x^3y - 4xy^3)$		
5	$(5z^3 - z)(x^5 - 10x^3y^2 + 5xy^4)$	67567.5	2.4892756
−5	$(5z^3 - z)(5x^4y - 10x^2y^3 + y^5)$		
6	$(15z^2 - 1)(x^6 - 15x^4y^2 + 15x^2y^4 - y^6)$	67567.5	0.3933012
−6	$(15z^2 - 1)(6x^5y - 20x^3y^3 + 6xy^5)$		
7	$z(x^7 - 21x^5y^2 + 35x^3y^4 - 7xy^6)$	2027025	2.2500000
−7	$z(7x^6y - 35x^4y^3 + 21x^2y^5 - y^7)$		
8	$x^8 - 28x^6y^2 + 70x^4y^4 - 28x^2y^6 + y^8$	2027025	0.6152344
−8	$8x^7y - 56x^5y^3 + 56x^3y^5 - 8xy^7$		

References

ALCOCK, N. W. (1970). *Crystallographic Computing*, edited by F. R. AHMED, S. R. HALL & C. P. HUBER, pp. 271–278. Copenhagen: Munksgaard.

BLESSING, R. H. (1989). *J. Appl. Cryst.* **22**, 396–397.

BOND, W. L. (1967). *International Tables for X-ray Crystallography*, Vol. II, edited by J. S. KASPER & K. LONSDALE, pp. 299–300, Table 5.3.6.*A*. Birmingham: Kynoch Press. (Present distributor Kluwer Academic Publishers, Dordrecht.)

BUSING, W. R. & LEVY, H. A. (1957). *Acta Cryst.* **10**, 180–182.

COPPENS, P. (1970). *Crystallographic Computing*, edited by F. R. AHMED, S. R. HALL & C. P. HUBER, pp. 255–270. Copenhagen: Munksgaard.

COPPENS, P., LEISEROWITZ, L. & RABINOVICH, D. (1965). *Acta Cryst.* **18**, 1035–1038.

DETITTA, G. T. (1985). *J. Appl. Cryst.* **18**, 75–79.

DUNITZ, J. D. (1979). *X-ray Analysis and the Structure of Organic Molecules*, p. 289. Ithaca, NY: Cornell Univ. Press.

DWIGGINS, C. W. JR (1975). *Acta Cryst.* A**31**, 395–396.

FLACK, H. D. (1974). *Acta Cryst.* A**30**, 569–573.

FLACK, H. D. (1977). *Acta Cryst.* A**33**, 890–898.

FLACK, H. D., VINCENT, M. G. & ALCOCK, N. W. (1980). *Acta Cryst* A**36**, 682–686.

HAMILTON, W. C. (1974). *International Tables for X-ray Crystallography*, Vol. IV, edited by W. C. HAMILTON & J. A. IBERS, pp. 273–284. Birmingham: Kynoch Press. (Present distributor Kluwer Academic Publishers, Dordrecht.)

HOWELLS, R. G. (1950). *Acta Cryst.* **3**, 366–369.

HUBER, R. & KOPFMAN, G. (1969). *Acta Cryst.* A**25**, 143–152.

KATAYAMA, C. (1986). *Acta Cryst.* A**42**, 19–23.

KOPFMAN, G. & HUBER, R. (1968). *Acta Cryst.* A**24**, 348–351.

MEULENAER, J. DE & TOMPA, H. (1965). *Acta Cryst.* **19**, 1014–1018.

NORTH, A. C. T., PHILLIPS, D. C. & MATHEWS, F. S. (1968). *Acta Cryst.* A**24**, 351–359.

PATURLE, A. (1990). Personal communication.

PATURLE, A. & COPPENS, P. (1988). *Acta Cryst.* A**44**, 6–7.

SOUHASSOU, M., ESPINOSA, E., LECOMTE, C. & BLESSING, R. H. (1995). *Acta Cryst.* Submitted.

WALKER, N. & STUART, D. (1983). *Acta Cryst.* A**39**, 158–166.

WELLS, M. (1960). *Acta Cryst.* **13**, 722–726.

WUENSCH, B. J. & PREWITT, C. T. (1965). *Z. Kristallogr.* **122**, 24–59.

Acta Cryst. (1995). A**51**, 38–47

A Matrix-Operator Approach to Reflection High-Energy Electron Diffraction Theory

BY PETER REZ

Center for Solid State Science and Department of Physics, Arizona State University, Tempe, AZ 85287–1704, *USA*

(*Received* 6 *April* 1994; *accepted* 13 *June* 1994)

Abstract

The amplitudes of beams reflected from a crystal surface by high-energy electrons are expressed in terms of matrix operators based on Bloch waves. The solution is derived in terms of the limiting case of an infinite slab and is therefore applicable to cases involving overlayers of different composition and

structure. The possibility of using a kinematical theory and its relationship to the full dynamical treatment are investigated. Calculations show that the method is limited by numerical problems but that it can be used to give a qualitative description of features in reflection high-energy electron diffraction.

Introduction

Reflection high-energy electron diffraction (RHEED) has become more important in recent years owing to the use of RHEED oscillations in monitoring the epitaxic growth of multilayer films (Neave, Dobson, Joyce & Zhang, 1985). There has also been increasing interest in using RHEED and reflection electron microscopy (REM) for the characterization of surface structure at the atomic level (Yagi, 1987). In those cases where RHEED is used to monitor film growth, a beam of energy between 10 and 30 kV is incident at a glancing angle of a few degrees. Generally, reflection electron microscopy is performed in electron microscopes and higher beam energies of 100 kV are used. The angle of incidence on the specimen is correspondingly smaller. In many respects, the theory of RHEED is similar to the theory for transmission electron diffraction or microscopy as exchange between the incident electron and the crystal electron can be neglected, unlike in low-energy electron diffraction (LEED). The boundary conditions are very different from the transmission electron diffraction case.

Many experimental surface scientists who use RHEED as a surface-characterization tool are quite satisfied with an analysis based on kinematic (single-scattering) theory (see, for example, Cohen, Petrich, Pukite, Whaley & Arrott, 1989). It is well known that electrons interact strongly with matter and strictly RHEED should be described by a multiple-scattering (dynamical) diffraction theory.

The first such theory of RHEED, based on Bloch waves, was published by Bethe (1928). Similar two-beam theories were developed by Kohra & Shinohara (1948), and Colella (1972) extended these ideas to the many-beam problem. An interesting diagonalization method based on the Hills determinant was proposed by Moon (1972). The Bloch-wave methods all rely on a three-dimensional Fourier analysis of the crystal potential. Peng (Peng & Whelan, 1990) has recently shown how to express the Bloch-wave theory in terms of matrix operators. He then applied the theory for one-rod systematic diffraction to the calculation of intensity of oscillations during epitaxic growth (Peng & Whelan, 1991*b*,*c*,*d*). Bloch-wave calculations have also been used to explain the phenomenon of surface resonance both numerically (Zuo & Liu, 1992) and analytically (Dudarev & Whelan, 1994).

In the last decade, it has become more common, following Maksym & Beeby (1981), to do a Fourier analysis in a plane parallel to the crystal surface and solve the coupled differential equations for propagation along the direction of the surface normal. Ichimiya (1983) has developed a variation of this method that uses matrix operators to represent the propagation through thin slabs. In these methods, it is implicitly assumed that the solution has decayed sufficiently so that a simple boundary condition can be imposed on the bottom surface of a crystal slab. However, there are still numerical problems as the exponentially growing solutions increase faster than the desired exponentially decaying solutions. Zhao, Poon & Tong (1988) have re-expressed the solution in terms of a logarithmic derivative that avoids many of the numerical problems of the Maksym & Beeby (1981) method. They argued that a large number of reciprocal-lattice rods were needed in the calculation for convergence. This was disputed by both Ichimiya (1990), who showed that his method converged with 11 rods, and Meyer-Ehmsen (1989), who separated the oscillatory behaviour from the reflection matrix and achieved convergence with seven rods for Pt(111). To achieve convergence for a wide range of angles in a rocking curve at an arbitrary azimuth, it is advisable to follow the prescription of Zhao, Poon & Tong (1988).

Finally, there have been calculations based on the transmission-microscopy multislice method (Peng & Cowley, 1986), which follows the propagation of the beam, as it travels through the crystal surface region. In effect, these calculations are applications of the standard transmission supercell method for crystal defects, where the defect is the crystal–vacuum interface. This would be called profile imaging in high-resolution microscopy of a thin specimen, with the beam incident on the surface plane. A disadvantage of these methods is that there are always questions on the magnitude of errors propagated and whether the solution has reached a steady state. The computer time is prohibitive for calculating rocking curves but the methods are very useful for calculating defect images in which there is no periodicity in the crystal surface plane.

If RHEED is to be applied routinely in determining surface structures, a simple quasikinematic interpretation of rocking-curve intensity distributions would be most useful. There has been much recent work on the GaAs(100) (2×4) reconstructed surface (Ma, Lordi, Larsen & Eades, 1993) and Knibb (1991) has made comparisons between dynamical and kinematic theories. Peng & Whelan (1991*a*) have suggested that it should be possible to treat the surface superlattice reflections kinematically. Korte & Meyer-Ehmsen (1993) have extended the calculation scheme used by Meyer-Ehmsen (1989) and con-

sider first-order diffuse scattering while retaining dynamical coupling between rods.

It is also necessary to have some method for exploring perturbations of atom positions, Debye–Waller factors or inelastic potentials in any attempt to solve the inverse problem. Both Peng (Peng & Whelan, 1992) and Stock & Meyer-Ehmsen (1990) have used nonlinear search procedures to determine best-fit parameters to describe the results of RHEED experiments. Peng & Dudarev (1993) have used a perturbation approach to calculate the changes of the specular beam intensity in a one-rod calculation for the Ni(001) p (2×2) surface when the top atom is displaced by up to 0.2 Å.

In this paper, a matrix form of RHEED theory is developed, similar to the coupled plane-wave equations of high-energy electron diffraction (Hirsch, Howie, Whelan, Nicholson & Pashley, 1965). The reflected-wave amplitudes are derived by applying the boundary conditions to a slab of thickness t and then allowing the thickness to tend to infinity. In this way, the exponentially growing solutions are formally eliminated. The various features of rocking curves are discussed and explained using simple quantum-mechanical models. Finally, the effect of perturbations are examined and the formal connection to a kinematic theory demonstrated. The applicability of various perturbations is also considered.

Theory

The behaviour of electrons at RHEED energies is governed by the Schrödinger equation

$$\frac{-\hbar^2}{2m}\left(\frac{\mathrm{d}^2\psi}{\mathrm{d}x^2}+\frac{\mathrm{d}^2\psi}{\mathrm{d}y^2}+\frac{\mathrm{d}^2\psi}{\mathrm{d}z^2}\right)+eV\psi=E\psi \qquad (1)$$

$$E=(\hbar^2/2m)(\chi_x^2+\chi_y^2+\chi_z^2), \qquad (2)$$

where χ_x, χ_y and χ_z are the components of the incident electron wave vector in free space. The x and y axes are in the surface plane and the z axis is along the surface normal directed into the crystal. Inside the crystal, the wave function is expanded as a three-dimensional Fourier series in terms of the reciprocal-lattice vectors,

$$\psi(r)=\sum_g \varphi_g(z)\exp[i(k_x+g_x)x + i(k_y+g_y)y+i(k_z+g_z)z], \qquad (3)$$

where k_x, k_y and k_z are the components of the wave vector in the crystal. Similarly, the potential is also expanded as a Fourier series:

$$U(\mathbf{r})=(2me/\hbar^2)V(\mathbf{r})=\sum_g U_g\exp(i\mathbf{g}\cdot\mathbf{r}). \qquad (4)$$

The continuity of the wave function and its derivative require that the x and y components of the electron wave vector match at the surface. This is true for all reciprocal-lattice rods labelled g_x, g_y:

$$\begin{aligned} k_x&=\chi_x \quad k_x+g_x=\chi_x+g_x \\ k_y&=\chi_y \quad k_y+g_y=\chi_y+g_y. \end{aligned} \qquad (5)$$

It is customary to include the mean inner potential in the definition of the z component of the wave vector:

$$k_z^2=\chi_z^2+U_{00}. \qquad (6)$$

The Schrödinger equation becomes

$$\frac{\mathrm{d}^2\varphi_g}{\mathrm{d}z^2}+2i(k_z+g_z)\frac{\mathrm{d}\varphi_g}{\mathrm{d}z}-[k_z^2+k_y^2+k_z^2-(k_z+g_z)^2 - (k_x+g_x)^2-(k_y+g_y)^2]\varphi_g+\sum_h U_{g-h}\varphi_h = 0, \qquad (7)$$

which can be expressed more compactly in matrix form as

$$\frac{\mathrm{d}}{\mathrm{d}z}\begin{pmatrix}\varphi\\ \mathrm{d}\varphi/\mathrm{d}z\end{pmatrix}=\begin{pmatrix}0 & \mathbf{I}\\ -\mathbf{Q} & -\mathbf{B}\end{pmatrix}\begin{pmatrix}\varphi\\ \mathrm{d}\varphi/\mathrm{d}z\end{pmatrix}, \qquad (8)$$

where

$$\begin{aligned} \mathbf{Q}_{gg}&=\mathbf{k}^2-(\mathbf{k}+\mathbf{g})^2\\ \mathbf{Q}_{gh}&=U_{g-h}\quad g\neq h\\ \mathbf{B}_{gg}&=2i(k_z+g_z)\\ \mathbf{B}_{gh}&=0\quad g\neq h. \end{aligned}$$

If a transformation is made such that $z'=iz$, the coupling matrix is purely real:

$$\frac{\mathrm{d}}{\mathrm{d}z'}\begin{pmatrix}\varphi\\ \mathrm{d}\varphi/\mathrm{d}z\end{pmatrix}=\begin{pmatrix}0 & \mathbf{I}\\ \mathbf{Q} & -\mathbf{B}\end{pmatrix}\begin{pmatrix}\varphi\\ \mathrm{d}\varphi/\mathrm{d}z'\end{pmatrix}. \qquad (9)$$

The solutions to the coupled differential equations can be found by diagonalizing the coupling matrix $\mathbf{L}$ in terms of the eigenvectors $\mathbf{C}$ and the eigenvalues $\boldsymbol{\lambda}$.

$$\mathbf{L}=\begin{pmatrix}0 & \mathbf{I}\\ -\mathbf{Q} & -\mathbf{B}\end{pmatrix} \qquad (10)$$

$$\mathbf{LC}=\mathbf{C}\boldsymbol{\lambda}$$

$$\begin{pmatrix}\varphi(t)\\ \mathrm{d}\varphi(t)/\mathrm{d}z\end{pmatrix}=\mathbf{C}[\exp(\boldsymbol{\lambda}t)]_D\,\mathbf{C}^{-1}\begin{pmatrix}\varphi(0)\\ \mathrm{d}\varphi(0)/\mathrm{d}z\end{pmatrix}. \qquad (11)$$

The coupling matrix, $\mathbf{L}$, has dimensions $2N\times2N$, where N is the number of Fourier coefficients in the expansion of the potential. The wavelength and its derivative at a depth t are now expressed in terms of the wavefunction and derivative at the entrance surface.

For the relevant boundary conditions to be applied, the solution must be reformulated in terms of the beams propagating in the vacuum outside the

crystal with wave vector

$$\chi_x + g_x,\ \chi_y + g_y,\ \pm[\chi^2 - (\chi_x + g_x)^2 - (\chi_y + g_y)^2]^{1/2}, \tag{12}$$

corresponding to each of the n reciprocal-lattice rods. The first point to note is that there are only $2n$ nondegenerate eigenvalues in the first Brillouin zone. These can be selected using a $2N \times 2n$ matrix $\mathbf{S}$ of the form

$$\mathbf{S} = \begin{pmatrix} 0 & 0 & 0 & \dots \\ 0 & 0 & 0 & \dots \\ 1 & 0 & 0 & \dots \\ 0 & 1 & 0 & \dots \\ 0 & 0 & 0 & \dots \\ \vdots & \vdots & \vdots & \ddots \end{pmatrix}. \tag{13}$$

It is also necessary to sum the amplitudes in the z direction along the foil normal. This can be achieved with a $2n \times 2N$ matrix $\mathbf{P}$ of the form

$$\mathbf{P} = \begin{pmatrix} 1 & \exp(ig_{2z}z) & \exp(ig_{3z}z) & 0 & 0 & 0 & 0 & \dots \\ 0 & 0 & 0 & 1 & \exp(ig_{2z}z) & 0 & 0 & \dots \\ 0 & 0 & 0 & 0 & 0 & 1 & \exp(ig_{2z}z) & \dots \\ \vdots & \vdots & \vdots & \vdots & \vdots & \vdots & \vdots & \ddots \end{pmatrix}. \tag{14}$$

The equation relating the wavefunction summed over the coefficients in a rod, Φ, and its derivative at depth, t, to that at the specimen surface can now be rewritten as

$$\begin{pmatrix} \boldsymbol{\Phi}(t) \\ \mathrm{d}\boldsymbol{\Phi}(t)/\mathrm{d}z \end{pmatrix} = \mathbf{P}\mathbf{C}\mathbf{S}[\exp(\boldsymbol{\lambda}t)]_D\mathbf{S}^T\mathbf{C}^{-1}\mathbf{P}^T \times \begin{pmatrix} \boldsymbol{\Phi}(0) \\ \mathrm{d}\boldsymbol{\Phi}(0)/\mathrm{d}z \end{pmatrix}. \tag{15}$$

The amplitudes of the beams in free space are denoted $\boldsymbol{\eta}_\pm$ and can be divided into forward and backward propagating parts according to the sign of the z component of the wave vector $\boldsymbol{\chi} = \pm[\chi^2 - (\chi_x + g_x)^2 - (\chi_y + g_y)^2]^{1/2}$. Matching wavefunctions at the exit surface of the crystal gives

$$\begin{aligned} \boldsymbol{\Phi}(z) &= \boldsymbol{\eta}_+ \exp(i\boldsymbol{\chi}_z z) + \boldsymbol{\eta}_- \exp(-i\boldsymbol{\chi}_z z) \\ \mathrm{d}\boldsymbol{\Phi}(z)/\mathrm{d}z &= i\boldsymbol{\chi}_z\boldsymbol{\eta}_+ \exp(i\boldsymbol{\chi}_z z) - i\boldsymbol{\chi}_z\boldsymbol{\eta}_- \exp(-i\boldsymbol{\chi}_z z), \end{aligned} \tag{16}$$

which can be expressed more conveniently in matrix form:

$$\begin{pmatrix} \boldsymbol{\Phi} \\ \mathrm{d}\boldsymbol{\Phi}/\mathrm{d}z \end{pmatrix} = \begin{pmatrix} \mathbf{I} & \mathbf{I} \\ i\boldsymbol{\chi}_z\mathbf{I} & -i\boldsymbol{\chi}_z\mathbf{I} \end{pmatrix} \begin{pmatrix} \boldsymbol{\eta}_+ \\ \boldsymbol{\eta}_- \end{pmatrix}. \tag{17}$$

The forward- and backward-propagating wave amplitudes can be expressed in terms of the Fourier-coefficient amplitudes by inverting (17):

$$\begin{pmatrix} \boldsymbol{\eta}_+ \\ \boldsymbol{\eta}_- \end{pmatrix} = \mathbf{F} \begin{pmatrix} \boldsymbol{\Phi} \\ \mathrm{d}\boldsymbol{\Phi}/\mathrm{d}z \end{pmatrix}, \tag{18}$$

where $\mathbf{F}$ is defined by

$$\mathbf{F} = \tfrac{1}{2} \begin{pmatrix} \mathbf{I} & \mathbf{I}/i\boldsymbol{\chi}_z \\ \mathbf{I} & -\mathbf{I}/i\boldsymbol{\chi}_z \end{pmatrix}. \tag{19}$$

Equation (15) becomes

$$\begin{pmatrix} \boldsymbol{\eta}_+(t) \\ \boldsymbol{\eta}_-(t) \end{pmatrix} = \mathbf{F}\mathbf{P}\mathbf{C}\mathbf{S}[\exp(\boldsymbol{\lambda}t)]_D\mathbf{S}^T\mathbf{C}^{-1}\mathbf{P}^T\mathbf{F}^{-1} \times \begin{pmatrix} \boldsymbol{\eta}_+(0) \\ \boldsymbol{\eta}_-(0) \end{pmatrix}. \tag{20}$$

To simplify (20), the matrix product $\mathbf{FPCS}$ is denoted $\mathbf{A}$ and its inverse $\mathbf{V}$. The eigenvalues can be separated into a set with positive real parts denoted $\boldsymbol{\lambda}$ and a corresponding set with negative real parts denoted $-\boldsymbol{\lambda}$. The forward- and backward-propagating waves can now be written as

$$\begin{pmatrix} \boldsymbol{\eta}_+(t) \\ \boldsymbol{\eta}_-(t) \end{pmatrix} = \begin{pmatrix} \mathbf{A}_{11} & \mathbf{A}_{12} \\ \mathbf{A}_{21} & \mathbf{A}_{22} \end{pmatrix} \begin{pmatrix} \exp(\boldsymbol{\lambda}t) & 0 \\ 0 & \exp(-\boldsymbol{\lambda}t) \end{pmatrix} \times \begin{pmatrix} \mathbf{V}_{11} & \mathbf{V}_{12} \\ \mathbf{V}_{21} & \mathbf{V}_{22} \end{pmatrix} \begin{pmatrix} \boldsymbol{\eta}_+(0) \\ \boldsymbol{\eta}_-(0) \end{pmatrix}. \tag{21}$$

Following the procedure used by Fathers & Rez (1979, 1984) in the solution of the electron-transport equation in semi-infinite specimens, the solution for the reflected wave at the surface, $\boldsymbol{\eta}_-(0)$, can be expressed in terms of the incident wave, $\boldsymbol{\eta}_+(0)$. As the thickness tends to infinity, the backward-propagating wave $\boldsymbol{\eta}_-(t)$ tends to zero. The reflected wave is given by

$$\begin{aligned} \boldsymbol{\eta}_-(0) = &-[\mathbf{A}_{21}\exp(\boldsymbol{\lambda}t)\,\mathbf{V}_{12} \\ &+ \mathbf{A}_{22}\exp(-\boldsymbol{\lambda}t)\mathbf{V}_{22}]^{-1}[\mathbf{A}_{21}\exp(\boldsymbol{\lambda}t)\,\mathbf{V}_{11} \\ &+ \mathbf{A}_{22}\exp(-\boldsymbol{\lambda}t)\,\mathbf{V}_{21}]\boldsymbol{\eta}_+(0). \end{aligned} \tag{22}$$

Extraction of a factor $\mathbf{A}_{21}\exp(\boldsymbol{\lambda}t)\mathbf{V}_{12}$ from the matrix operator that is being inverted leads to

$$\begin{aligned}\boldsymbol{\eta}_-(0) = &-[I + \mathbf{V}_{12}^{-1}\exp(-\boldsymbol{\lambda}t)\mathbf{A}_{21}^{-1}\mathbf{A}_{22} \\ &\times \exp(-\boldsymbol{\lambda}t)\,\mathbf{V}_{22}]^{-1}\mathbf{V}_{12}^{-1}\exp(-\boldsymbol{\lambda}t)\,\mathbf{A}_{21}^{-1} \\ &\times [\mathbf{A}_{21}\exp(\boldsymbol{\lambda}t)\,\mathbf{V}_{11} \\ &+ \mathbf{A}_{22}\exp(-\boldsymbol{\lambda}t)\,\mathbf{V}_{21}]\boldsymbol{\eta}_+(0). \qquad (23)\end{aligned}$$

As t tends to infinity, we are left with

$$\boldsymbol{\eta}_-(0) = -\mathbf{V}_{12}^{-1}\mathbf{V}_{11}\,\boldsymbol{\eta}_+(0), \qquad (24)$$

which can be rewritten as

$$\boldsymbol{\eta}_-(0) = \mathbf{A}_{22}\mathbf{A}_{12}^{-1}\boldsymbol{\eta}_+(0) \qquad (25)$$

by making use of the fact that $\mathbf{V}$ is the inverse of $\mathbf{A}$.

This result is identical to that which would have been obtained by excluding Bloch waves that correspond to exponentially growing solutions. In terms of Bloch-wave coefficients α_j, the wave function in the crystal can be written as

$$\begin{aligned}\psi(\mathbf{r}) = &\sum_{g_x,g_y}\sum_{g_z,j}\alpha_j C_g^j \exp[i(\gamma_j + k_z + g_z)z] \\ &\times \exp[i(k_x + g_x)x + (k_y + g_y)y], \qquad (26)\end{aligned}$$

where γ_j are the eigenvalues of the matrix $\mathbf{L}$. In terms of the amplitudes for the rods designated by $g_{x,y}$, the wave function outside the crystal is

$$\eta_{g_{x,y}}^+(0)\exp(i\chi_{g_{x,y}}z) + \eta_{g_{x,y}}^-(0)\exp(-i\chi_{g_{x,y}}z). \qquad (27)$$

Application of the boundary condition leads to

$$\sum_{g_z,j}\alpha_j C_g^j = \eta_{g_{x,y}}^+(0) + \eta_{g_{x,y}}^-(0) \qquad (28a)$$

$$\sum_{g_z,j}\alpha_j C_g^j(\gamma_j + k_z + g_z) = \chi_{g_{x,y}}\eta_{g_{x,y}}^+(0) - \chi_{g_{x,y}}\eta_{g_{x,y}}^-(0). \qquad (28b)$$

The reflected amplitudes can be solved as

$$\begin{aligned}\eta_{g_{x,y}}^-(0) = &\left\{\sum_{g_z,j} C_g^j - \sum_{g_z,j} C_g^j[(\gamma_j + k_z + g_z)/\chi_{g_{x,y}}]\right\} \\ &\times \left\{\sum_{g_z,j} C_g^j + \sum_{g_z,j} C_g^j \right. \\ &\left.\times [(\gamma_j + k_z + g_z)/\chi_{g_{x,y}}]\right\}^{-1}\eta_{g_{x,y}}^+(0). \qquad (29)\end{aligned}$$

The term in the first bracket can be identified with $\mathbf{A}_{22}$ and the second term with $\mathbf{A}_{12}{}^{-1}$.

Overlayers

The reflected amplitudes for a system with a layer of thickness t on a semi-infinite bulk slab can be formally derived from (20) and (21). Equation (25) or (29) describes the scattering from the semi-infinite bulk medium. For convenience, this is rewritten as

$$\boldsymbol{\eta}_-(t) = \mathbf{R}_B\boldsymbol{\eta}_+(t), \qquad (30)$$

where R_B is the reflection matrix of the bulk. Equation (20) or (21) applies for scattering by the thin overlayer. Equation (21) is expressed as

$$\begin{pmatrix}\boldsymbol{\eta}_+(t) \\ \boldsymbol{\eta}_-(t)\end{pmatrix} = \begin{pmatrix}\mathbf{T}_{11}(t) & \mathbf{T}_{12}(t) \\ \mathbf{T}_{21}(t) & \mathbf{T}_{22}(t)\end{pmatrix}\begin{pmatrix}\boldsymbol{\eta}_+(0) \\ \boldsymbol{\eta}_-(0)\end{pmatrix}, \qquad (31)$$

where the matrices $T_{ij}(t)$ can be calculated from A_{ij}, V_{ij} and $\exp(\lambda t)$. The expression for the reflected amplitudes from the layer and bulk slab is

$$\begin{aligned}\boldsymbol{\eta}_-(0) = &[\mathbf{T}_{21}(t) + \mathbf{T}_{22}(t)\mathbf{R}_B] \\ &\times [\mathbf{T}_{11}(t) + \mathbf{T}_{12}(t)\mathbf{R}_B]^{-1}\boldsymbol{\eta}_+(0). \qquad (32)\end{aligned}$$

Again, in accord with Fathers & Rez (1979, 1984), the $T_{ij}(t)$ matrices could all be calculated using decaying exponentials, though this should not be necessary for RHEED problems involving layers with a thickness of only a few atomic planes. For a thin layer, the Fourier-series expansion of (3) and (4) should be replaced by a Fourier transform by making g_z a continus variable. Using the Fourier-series representation is equivalent to doing a Fourier integral by summing over the values of the potential sampled at discrete reciprocal-lattice vectors. Approximating an atom as a Gaussian of half-width 0.5 Å gives a maximum fractional error in the potential of 20%. The error would be most serious at glancing angles where the details of the potential have the greatest effect.

Perturbation theory

To examine the relationship between the full dynamical theory and a kinematic theory, it is useful to develop a perturbation theory for the reflected-beam amplitudes. It is convenient to assume that there is only one Fourier coefficient of potential for each rod, and that those Fourier coefficients of potential U_{g-h} representing coupling between rods can be considered small compared with U_{00}. The matrix $\mathbf{Q}$ in (8) is now diagonal and for each rod a Schrödinger equation such as (A1) in the Appendix applies, with complex wave vector λ given by $\alpha + i\beta$. The off-diagonal parts of the original matrix $\mathbf{M}$, given in (8), can be considered as a perturbing matrix, $\mathbf{U}$.

The eigenvector matrix for the unperturbed case is

$$\mathbf{C} = \begin{pmatrix}\mathbf{I} & \mathbf{I} \\ i\boldsymbol{\lambda} & -i\boldsymbol{\lambda}\end{pmatrix}. \qquad (33)$$

Standard perturbation theory gives the perturbed

eigenvector matrix as $\mathbf{C}(\mathbf{I}+\mathbf{B})$,

$$B_{gh}-\tfrac{1}{2}\begin{pmatrix}\dfrac{U_{gh}}{\lambda_g(\lambda_h-\lambda_g)} & \dfrac{-U_{gh}}{\lambda_g(\lambda_h+\lambda_g)}\\ \dfrac{-U_{gh}}{\lambda_g(\lambda_h+\lambda_g)} & \dfrac{U_{gh}}{\lambda_g(\lambda_h-\lambda_g)}\end{pmatrix}. \tag{34}$$

The matrix operator representing scattering from a layer of thickness t, following (15), can be written as

$$\boldsymbol{\phi}(t)=\mathbf{C}(\mathbf{I}+\mathbf{B})\exp(i\boldsymbol{\lambda}t)(\mathbf{I}-\mathbf{B})\mathbf{C}^{-1}\boldsymbol{\phi}(0) \tag{35}$$

$$\boldsymbol{\phi}(t)=\{\mathbf{C}\exp(i\boldsymbol{\lambda}t)\mathbf{C}^{-1}+\mathbf{C}[\mathbf{B}\exp(i\boldsymbol{\lambda}t)-\exp(i\boldsymbol{\lambda}t)\mathbf{B}]\mathbf{C}^{-1}\}\boldsymbol{\phi}(0). \tag{36}$$

The amplitudes in the slice, $\boldsymbol{\phi}$, can be transformed into the reflected and transmitted amplitudes, $\boldsymbol{\eta}$, using the operator $\mathbf{F}$ from (19). The product $\mathbf{D}=\mathbf{F}\,\mathbf{C}$ is given by

$$\mathbf{D}=\tfrac{1}{2}\begin{pmatrix}\mathbf{I}+(\boldsymbol{\lambda}/\boldsymbol{\chi}) & \mathbf{I}-(\boldsymbol{\lambda}/\boldsymbol{\chi})\\ \mathbf{I}-(\boldsymbol{\lambda}/\boldsymbol{\chi}) & \mathbf{I}+(\boldsymbol{\lambda}/\boldsymbol{\chi})\end{pmatrix} \tag{37a}$$

and the inverse is

$$\mathbf{D}^{-1}=\tfrac{1}{2}\begin{pmatrix}\mathbf{I}+(\boldsymbol{\chi}/\boldsymbol{\lambda}) & \mathbf{I}-(\boldsymbol{\chi}/\boldsymbol{\lambda})\\ \mathbf{I}-(\boldsymbol{\chi}/\boldsymbol{\lambda}) & \mathbf{I}+(\boldsymbol{\chi}/\boldsymbol{\lambda})\end{pmatrix}, \tag{37b}$$

where χ are the wave vectors in free space. The amplitudes from the slice are now given by

$$\boldsymbol{\eta}(t)=\{\mathbf{D}\exp(i\boldsymbol{\lambda}t)\mathbf{D}^{-1}+\mathbf{D}[\mathbf{B}\exp(i\boldsymbol{\lambda}t)-\exp(i\boldsymbol{\lambda}t)\mathbf{B}]\mathbf{D}^{-1}\}\boldsymbol{\eta}(0). \tag{38}$$

If it is assumed that U_{00} is zero, then the matrix $\mathbf{D}$ is the unit matrix and the effects of the perturbing potential, $\mathbf{U}$, are given by the second term in square brackets, $\mathbf{M}$, whose components are

$$\mathbf{M}=\tfrac{1}{2}\begin{pmatrix}\dfrac{U_{gh}[\exp(i\chi_h t)-\exp(i\chi_g t)]}{\chi_g(\chi_h-\chi_g)} & \dfrac{-U_{gh}[\exp(-i\chi_h t)-\exp(i\chi_g t)]}{\chi_g(\chi_h+\chi_g)}\\ \dfrac{-U_{gh}[\exp(-i\chi_h t)-\exp(-i\chi_g t)]}{\chi_g(\chi_h+\chi_g)} & \dfrac{U_{gh}[\exp(-i\chi_h t)-\exp(-i\chi_g t)]}{\chi_g(\chi_h-\chi_g)}\end{pmatrix}. \tag{39}$$

Equation (38) simplifies to

$$\begin{pmatrix}\boldsymbol{\eta}_+(t)\\ \boldsymbol{\eta}_-(t)\end{pmatrix}=\begin{pmatrix}\exp(i\boldsymbol{\chi}t)+\mathbf{M}_{11} & \mathbf{M}_{12}\\ \mathbf{M}_{21} & \exp(-i\boldsymbol{\chi}t)+\mathbf{M}_{22}\end{pmatrix}\begin{pmatrix}\boldsymbol{\eta}_+(0)\\ \boldsymbol{\eta}_-(0)\end{pmatrix}. \tag{40}$$

The reflected amplitude at the surface can now be written as

$$[\mathbf{R}_B\exp(i\boldsymbol{\chi}t)+\mathbf{R}_B\mathbf{M}_{11}-\mathbf{M}_{21}]\boldsymbol{\eta}_+(0)=[\exp(-i\boldsymbol{\chi}t)+\mathbf{M}_{22}-\mathbf{R}_B\mathbf{M}_{12}]\boldsymbol{\eta}_-(0), \tag{41}$$

where $\mathbf{R}_B$ is the corresponding amplitude vector for the bulk alone. The reflection amplitude operator for the thin layer and bulk is

$$\mathbf{R}=-[\exp(-i\boldsymbol{\chi}t)+\mathbf{M}_{22}-\mathbf{R}_B\mathbf{M}_{12}]^{-1}\times[\mathbf{R}_B\exp(i\boldsymbol{\chi}t)+\mathbf{R}_B\mathbf{M}_{11}-\mathbf{M}_{21}], \tag{42}$$

which can be expanded to first order in the perturbing matrix $\mathbf{M}$,

$$\begin{aligned}\mathbf{R}=&\exp(i\boldsymbol{\chi}t)\,\mathbf{R}_B\exp(i\boldsymbol{\chi}t)\\ &-\exp(i\boldsymbol{\chi}t)\mathbf{M}_{22}\exp(i\boldsymbol{\chi}t)\mathbf{R}_B\exp(i\boldsymbol{\chi}t)\\ &+\exp(i\boldsymbol{\chi}t)\mathbf{R}_B\mathbf{M}_{11}-\exp(i\boldsymbol{\chi}t)\mathbf{M}_{21}\\ &+\exp(i\boldsymbol{\chi}t)\mathbf{R}_B\mathbf{M}_{12}\exp(i\boldsymbol{\chi}t)\mathbf{R}_B\exp(i\boldsymbol{\chi}t).\end{aligned} \tag{43}$$

The first term can be identified with transmission through the thin slice, reflection in the bulk and then transmission back through the slice. The second term corresponds to reflection from the bulk followed by kinematic scattering in the slice, while the third term corresponds to kinematic scattering in the slice followed by reflection from the bulk. The fourth term corresponds to a single kinematic reflection in the slice and is smaller than the second and third terms as a larger reciprocal-lattice vector is involved. The last term represents a reflection from the bulk followed by a kinematic reflection in the slice that is then reflected by the bulk. As it is of higher order than the other terms in (43), it is neglected.

Results

In reflection electron diffraction, it is customary to record data as rocking curves, which show the intensity in a given beam as a function of the angle of incidence. A program was written based on (25) for calculating reflected intensities. The potentials were calculated from the X-ray scattering factors of Doyle & Turner (1968) using the Mott formula, and the non-Hermitian part was calculated using the program given by Bird (Bird & King, 1990). The fundamental shape of the rocking curve can be understood by examining the analytical form of the reflected intensity from a barrier with a complex potential as given in the Appendix. In the region

Table 1. *Parameters used in the calculations*

	Fig. 1	Fig. 2(*a*)	Fig. 2(*b*)	Fig. 3	Figs. 4 & 5
Surface	Pt(111)	Ag(002)	MgO(002)	Pt(002)	GaAs(002)
Azimuth	$2\bar{1}1$	110	010	010	$\bar{2}20$
Rods and no. of Fourier coefficients	000 (9)	000 (7) $\pm 2\bar{2}0$ (5) $\pm 4\bar{4}0$ (3)	000 (7) ± 200 (5) ± 400 (3)	000 (9) ± 200 (7)	000 (9) ± 220 (7)
V_0 (eV)	30	24	18	30	14.5
V_0' (eV)	2.0	3.0	1.0	15.0	10.0
u^2 (Å^2)	0.0	0.0	0.3	0.19	0.41
Voltage (kV)	20	20	10	20	13

where k_z is less than $2meV/\hbar^2$, there is total reflection. For high angles of incidence, the reflected intensity varies as given by (*A*7). Making the potential periodic normal to the surface introduces peaks at the Bragg angles as shown in Fig. 1 for the Pt(111) row with nine coefficients of potential. The accelerating voltage was 20 kV, which would give successive peaks at 1.2°.

The behaviour is further complicated when three-dimensional diffraction is introduced. The rocking curves for the (002) surfaces of silver at 20 kV and MgO at 10 kV are shown in Figs. 2(*a*) and (*b*), respectively. These were all three-rod calculations where the 000 rod is shown as a solid line, while the $2\bar{2}0$ rod for silver and the 200 rod for MgO are shown as dashed lines. The exact conditions are given in Table 1.

The program was modified using (32) to calculate the reflected intensity for an overlayer on a substrate. The effects of various overlayers were explored with three-rod calculations using parameters given in Table 1. Owing to the approximate sampling of the variation in the potential in the z direction, the results should only be used for a qualitative interpretation of the effects on RHEED intensity. Fig. 3 shows the results for an overlayer on Pt (002) that was stretched by 10%. The outer-atom positions were also moved 0.04 Å inwards, though this did not affect the results. The rocking curve is also shown for a bulk crystal that is stretched in the [001] direction by 10%. The peaks shift to new positions, as would be expected from the change in Bragg angle, and there is not much difference between bulk specimen and a single overlayer. This indicates that RHEED is dominated by scattering in single layers. A similar result is shown in Fig. 4(*a*) for GaAs(002), where the surface layer is stetched 10%, the outer Ga atoms are moved inwards 0.28 Å and the As atoms are moved 0.14 Å in the same direction. The rocking curve from GaAs with an overlayer is compared with that from the bulk crystal in Fig. 4(*a*). In Fig. 4(*b*), the GaAs

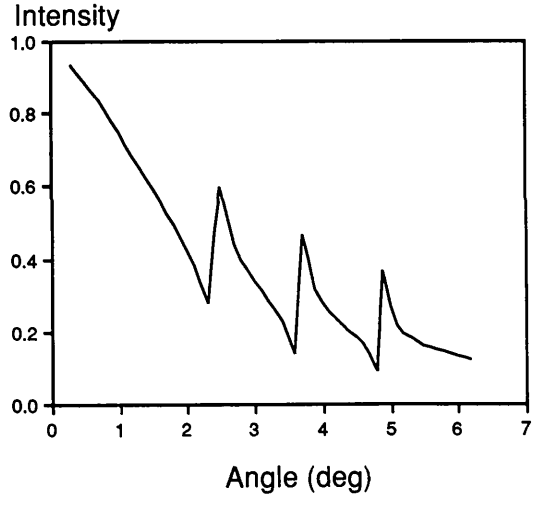

Fig. 1 Rocking curve for Pt(111) at 20 kV.

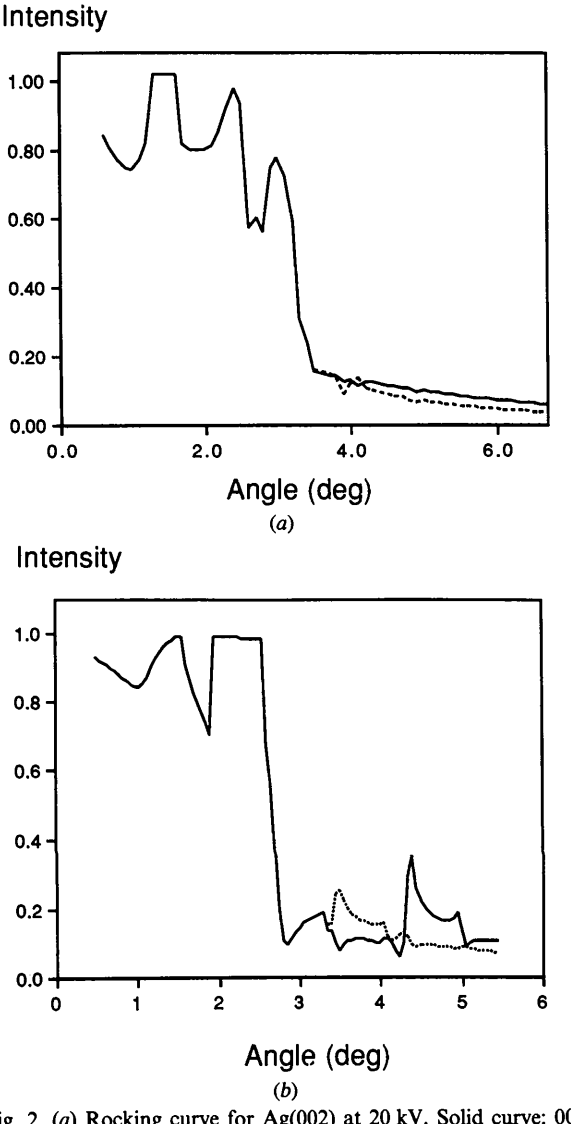

Fig. 2. (*a*) Rocking curve for Ag(002) at 20 kV. Solid curve: 000 rod; dashed curve: $2\bar{2}0$ rod. (*b*) Rocking curve for MgO(002) at 10 kV. Solid curve: 000 rod; dashed curve: 200 rod.

rocking curve is compared with the corresponding rocking curve from a bulk material where the unit cell is stretched by 10% in the [002] direction but the relative atom positions are unchanged. The main effect on the rocking curves comes about from stretching the layer, which changes the Bragg angles, though the atom-position-shift changes the relative heights of peaks between 2.5 and 3°. In another calculation (Fig. 5), the effects of replacing the top layer with a layer of AlAs are shown. The rocking curves are different over the entire angular range and the high-angle part with the AlAs layer shows intensity oscillations with angle (Fig. 5*b*). The 220 rod for the AlAs overlayers follows the same form as the bulk GaAs but is lower in intensity (Fig. 5*c*).

Various calculations were attempted that treated the difference between an overlayer and the substrate as a perturbation and used (42), which represents single scattering, and (43), which is similar and represents first-order perturbation theory. The results were disappointing and gave neither the correct magnitude nor the functional form of the rocking curve. Although it would be convenient if RHEED in some form could be calculated kinematically, it appears that even in a single layer strong dynamical multiple-scattering effects have to be considered, as has been suggested by Meyer-Ehmsen (1989), Peng (Peng & Cowley, 1986) and others. The RHEED theory given above is probably not the best way of doing practical calculations. Even for calculations with relatively few rods, the matrix that must be diagonalized in (10) becomes large enough ($> 50 \times 50$) that serious errors occur in the diagonalization procedure. The scaling of diagonalization time as N^3 also has to be considered. The optimal method for rocking-curve calculations is probably a modified form of that proposed by Maksym & Beeby (1981) as published by Meyer-Ehmsen (1989). It would be interesting to see how some of the perturbation-theory techniques proposed in this paper relate to the first-order diffuse scattering theory given by Korte & Meyer-Ehmsen (1993).

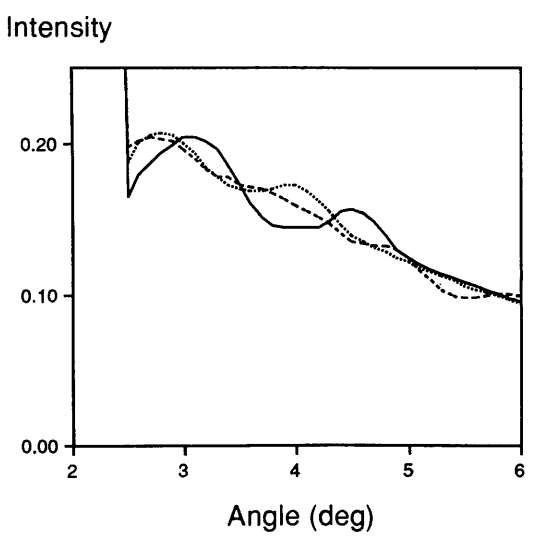

Fig. 3. Rocking curve for Pt(002) 000 rod at 20 kV (solid curve). Dashed curve: overlayer stretched 10% in [002] direction. Dotted curve: bulk with lattice stretched 10% in [002] direction.

Concluding remarks

A theory of RHEED is developed in terms of matrix operators where the reflected amplitude is explicitly derived as the limiting case for a semi-infinite slab. The theory is generalized for overlayers and the relationship between kinematic theory and a first-

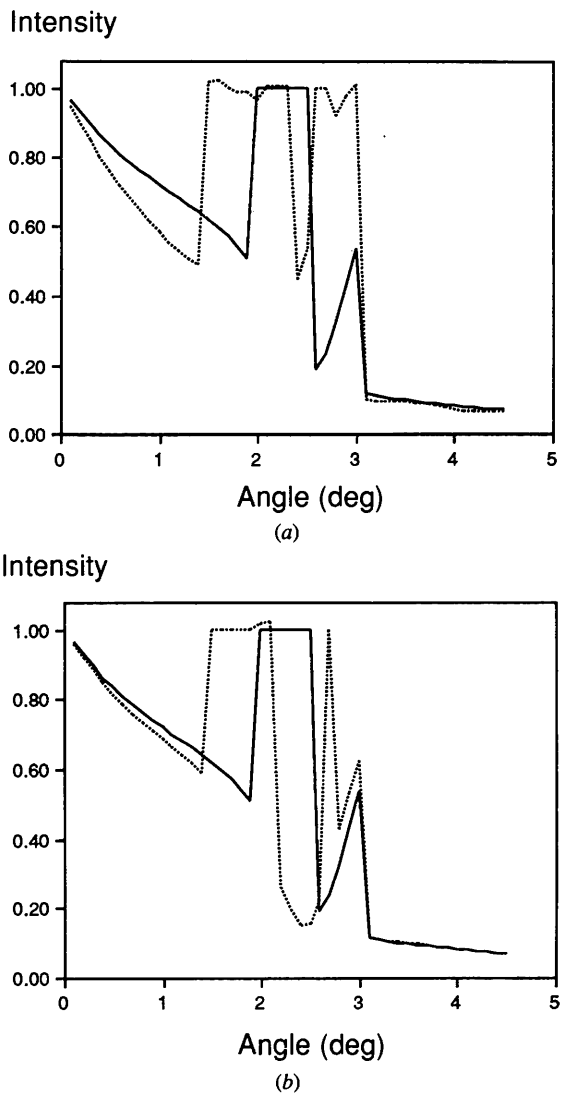

Fig. 4. (*a*) Rocking curve for GaAs(002) 000 rod at 13 kV (solid curve). Dashed curve: overlayer modified as described in text. (*b*) Solid curve as in (*a*). Dashed curve: bulk with unit cell the same as the overlayer in (*a*).

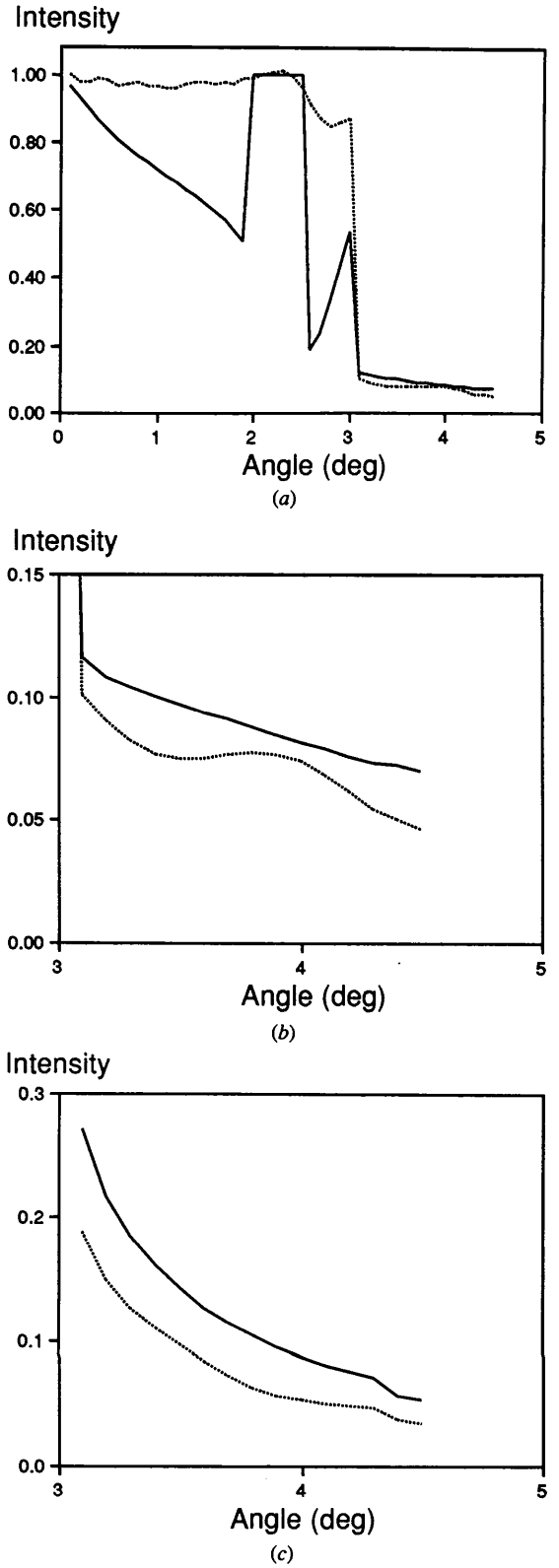

Fig. 5. (*a*) Rocking curve for GaAs(002) 000 rod at 13 kV (solid curve). Dotted curve: AlAs overlayer. (*b*) High-angle portion of (*a*). (*c*) Rocking curve for 220 rod. Solid curve: GaAs(002) surface; dotted curve: AlAs overlayer on GaAs(002).

order perturbation treatment is explored. The kinematic theory is shown to be identical to first-order perturbation theory for a layer when only terms corresponding to single scattering before or after a reflection from the bulk are considered. The general form of the reflected-intensity rocking curve is discussed in terms of reflection from a potential barrier and the one-rod case. Calculations are also presented showing the results for various overlayers. Stretching the overlayer can cause changes in peak positions due to changes in effective Bragg angles. Displacing atoms within the overlayer may give changes in relative peak intensities. Calculations show that RHEED is strongly dynamical, even within the surface layer. Owing to the limited number of rods in these calculations and the approximate sampling of the potential variation for overlayers, the results of this method can only be used for a qualitative interpretation of RHEED features. Kinematical or single-scattering calculations using just the difference between the overlayer and the bulk fail to give either the correct magnitude of intensity in the rocking curve or even the correct functional form. Owing to numerical diffculties with diagonalizing large matrices, it is suggested that the method proposed by Meyer-Ehmsen (1989) and that of Zhao *et al.* (1988) are better suited to realistic RHEED calculations.

I thank Drs A. Bleloch and J. M. Zuo for many stimulating dicussions and for allowing me to compare my results with their programs. I also thank Professors A. Howie and L. M. Brown for their hospitality during my stay at the Cavendish Laboratory. Some of the calculations used computing facilities at the National Center for High-Resolution Microscopy, funded by the NSF as grant DMR 91-15680.

APPENDIX

To understand the properties of the specularly reflected wave, it is useful to examine the reflection from a region with an arbitrary complex potential. The Schrödinger equation is

$$-(\hbar^2/2m)\nabla^2\psi + e(V_r + iV_i)\psi = E\psi, \qquad (A1)$$

which for this one-dimensional problem can be rewritten as

$$d^2\psi/dz^2 = -[(\chi^2 + U_r) + iU_i]\psi. \qquad (A2)$$

The solutions are waves with wave vectors $\pm(\alpha \pm i\beta)$, where α and β are given by

$$\alpha = [(\chi^2 + U_r)/2]^{1/2}(1 + \{1 + [U_i^2/(\chi^2 + U_r)]\}^{1/2})^{1/2} \qquad (A3a)$$

$$\beta = [(\chi^2 + U_r)/2]^{1/2}(\{1 + [U_i^2/(\chi^2 + U_r)]\}^{1/2} - 1)^{1/2}. \qquad (A3b)$$

If U_i is much less than $\chi^2 + U_r$, then α and β can be approximated as

$$\alpha = (\chi^2 + U_r)^{1/2}[1 + \tfrac{1}{8}(U_i^2/U_r^2)], \quad (A4a)$$

$$\beta = U_i/2(\chi^2 + U_r)^{1/2}. \quad (A4b)$$

The reflected amplitude, R, can be solved by matching the boundary conditions.

$$R = (\chi - \alpha - i\beta)/(\chi + \alpha + i\beta). \quad (A5)$$

In the limit of small K or for $\chi^2 < U_r$, the reflected amplitude is unity. For large χ (corresponding to a large angle for the specular beam) it can be approximated as

$$R = iU_i/4\chi^2, \quad (A6)$$

which only depends strongly on the imaginary part of the potential. The reflected intensity is therefore

$$I = U_i^2/16\chi^4. \quad (A7)$$

References

BETHE, H. (1928). *Ann Phys. (Leipzig)*, **87**, 55–69.
BIRD, D. M. & KING, Q. A. (1990). *Acta Cryst.* A**46**, 202–208.
COHEN, P. I., PETRICH, G. S., PUKITE, P. R., WHALEY, G. J. & ARROTT, A. S. (1989). *Surf. Sci.* **216**, 222–248.
COLELLA, R. (1972). *Acta Cryst.* A**28**, 11–15.
DOYLE, P. A. & TURNER, P. S. (1968). *Acta Cryst.* A**24**, 390–397.
DUDAREV, S. L. & WHELAN, M. J. (1994). *Phys. Rev. Lett.* **72**, 1032–1035.
FATHERS, D. J. & REZ, P. (1979). *Scanning Electron Microscopy* 1, pp. 55–66. O'Hare: SEM Inc.
FATHERS, D. J. & REZ, P. (1984). *Electron Beam Interactions with Solids*, pp. 193–208. O'Hare: SEM Inc.
HIRSCH, P. B., HOWIE, A., WHELAN, M. J., NICHOLSON, R. B. & PASHLEY, D. W. (1965). *Electron Microscopy of Thin Crystals*. London: Butterworths.
ICHIMIYA, A. (1983). *Jpn. J. Appl. Phys.* **22**, 176–180.
ICHIMIYA, A. (1990). *Surf. Sci.* **235**, 75–83.
KNIBB, M. G. (1991). *Surf. Sci.* **257**, 389–401.
KOHRA, K. & SHINOHARA, K. (1948). *J. Phys. Soc. Jpn*, **4**, 155–160.
KORTE, U. & MEYER-EHMSEN, G. (1993). *Phys. Rev. B*, **48**, 8345–8355.
MA, Y., LORDI, S., LARSEN, P. K. & EADES, J. A. (1993). *Surf. Sci.* **289**, 47–67.
MAKSYM, P. A. & BEEBY, J. L. (1981). *Surf. Sci.* **110**, 423–438.
MEYER-EHMSEN, G. (1989). *Surf. Sci.* **219** 177–188.
MOON, A. R. (1972). *Z. Naturforsch.* **27**, 391–395.
NEAVE, J. H., DOBSON, P. J., JOYCE, B. A. & ZHANG, J. (1985). *Appl. Phys. Lett.* **47**, 100–102.
PENG, L.-M. & COWLEY, J. M. (1986). *Acta Cryst.* A**42**, 545–552.
PENG, L.-M. & DUDAREV, S. L. (1993). *Surf. Sci.* **298**, 316–330.
PENG, L.-M. & WHELAN, M. J. (1990). *Proc. R. Soc. London Ser. A*, **431**, 125–142.
PENG, L.-M. & WHELAN, M. J. (1991*a*). *Acta Cryst.* A**47**, 95–101.
PENG, L.-M. & WHELAN, M. J. (1991*b*). *Proc. R. Soc. London Ser. A*, **432**, 195–213.
PENG, L.-M. & WHELAN, M. J. (1991*c*). *Proc. R. Soc. London Ser. A*, **435**, 257–267.
PENG, L.-M. & WHELAN, M. J. (1991*d*). *Proc. R. Soc. London Ser. A*, **435**, 269–286.
PENG, L.-M. & WHELAN, M. J. (1992). *Surf. Sci. Lett.* **268**, L325–L329.
STOCK, M. & MEYER-EHMSEN, G. (1990). *Surf. Sci. Lett.* **226**, L59–L62.
YAGI, K. (1987). *J. Appl. Cryst.* **20**, 147–160.
ZHAO, T. C., POON, H. C. & TONG, S. Y. (1988). *Phys. Rev. B*, **38**, 1172–1195.
ZUO, J. M. & LIU, J. (1992). *Surf. Sci.* **271**, 253–259.

Acta Cryst. (1995). A**51**, 47–53

On the Single-Pixel Approximation in Maximum-Entropy Analysis

BY SHINTARO KUMAZAWA

Department of Physics, Science University of Tokyo, Chiba, 278 *Japan*

AND MASAKI TAKATA AND MAKOTO SAKATA

Department of Applied Physics, Nagoya University, Nagoya, 464 *Japan*

(*Received* 21 *June* 1993; *accepted* 31 *May* 1994)

Abstract

By a recent development of the maximum-entropy method (MEM) following Sakata & Sato [*Acta Cryst.* (1990), A**46**, 263–270], electron- (or nuclear-) density distributions have been obtained for crystalline materials of simple structures from single-crystal or powder diffraction data. In order to obtain a ME density map, the ME equation is solved iteratively under the zeroth-order single-pixel approximation (ZSPA) starting from the uniform density. The purpose of this paper is to examine the validity of the ZSPA by using a one-dimensional two-pixel model for which the exact solution can be analytically obtained. For this model, it is also possible to solve the ME equation numerically without ZSPA by the same iterative procedure as in the case of ZSPA. By comparison of these three solutions for a one-